

The Bain library: A Cu-Au buffer template for a continuous variation of lattice parameters in epitaxial films

S. Kauffmann-Weiss, S. Hamann, L. Reichel, A. Siegel, V. Alexandrakis, R. Heller, L. Schultz, A. Ludwig, and S. Fähler

Citation: [APL Materials](#) **2**, 046107 (2014); doi: 10.1063/1.4870759

View online: <https://doi.org/10.1063/1.4870759>

View Table of Contents: <http://aip.scitation.org/toc/apm/2/4>

Published by the [American Institute of Physics](#)

Articles you may be interested in

[Two-dimensional electron gas in monolayer InN quantum wells](#)

Applied Physics Letters **105**, 213503 (2014); 10.1063/1.4902916

[Formation and propagation of laser-driven plasma jets in an ambient medium studied with X-ray radiography and optical diagnostics](#)

Physics of Plasmas **22**, 012702 (2015); 10.1063/1.4905525

[Tuning of the nucleation field in nanowires with perpendicular magnetic anisotropy](#)

Journal of Applied Physics **113**, 163902 (2013); 10.1063/1.4802687

[Fabrication of nanopores in 1 nm thick carbon nanomembranes with slow highly charged ions](#)

Applied Physics Letters **102**, 063112 (2013); 10.1063/1.4792511

[Analytical solution for the diffusion of a capacitor discharge generated magnetic field pulse in a conductor](#)

AIP Advances **6**, 065014 (2016); 10.1063/1.4954400

[Shapeable magnetoelectronics](#)

Applied Physics Reviews **3**, 011101 (2016); 10.1063/1.4938497

PHYSICS TODAY

WHITEPAPERS

ADVANCED LIGHT CURE ADHESIVES

Take a closer look at what these environmentally friendly adhesive systems can do

READ NOW

PRESENTED BY
 **MASTERBOND**
ADHESIVES | SEALANTS | COATINGS

The Bain library: A Cu-Au buffer template for a continuous variation of lattice parameters in epitaxial films

S. Kauffmann-Weiss,^{1,2,3,4,a} S. Hamann,¹ L. Reichel,^{2,3} A. Siegel,¹
 V. Alexandrakis,¹ R. Heller,⁵ L. Schultz,^{2,3} A. Ludwig,¹ and S. Fähler^{2,4}

¹Ruhr-University Bochum, Faculty of Mechanical Engineering, Institute for Materials, 44801 Bochum, Germany

²IFW Dresden, P.O. Box 270116, 01171 Dresden, Germany

³Dresden University of Technology, Institute for Materials Science, 01062 Dresden, Germany

⁴Technische Universität Chemnitz, Faculty of Natural Science, Institute of Physics, 09107 Chemnitz, Germany

⁵Helmholtz-Zentrum Dresden-Rossendorf, P.O. Box 510119, 01314 Dresden, Germany

(Received 22 November 2013; accepted 27 March 2014; published online 10 April 2014)

Smallest variations of the lattice parameter result in significant changes in material properties. Whereas in bulk, lattice parameters can only be changed by composition or temperature, coherent epitaxial growth of thin films on single crystals allows adjusting the lattice parameters independently. Up to now only discrete values were accessible by using different buffer or substrate materials. We realize a lateral variation of in-plane lattice parameters using combinatorial film deposition of epitaxial Cu-Au on a 4-in. Si wafer. This template gives the possibility to adjust the in-plane lattice parameter over a wide range from 0.365 nm up to 0.382 nm. © 2014 Author(s). All article content, except where otherwise noted, is licensed under a Creative Commons Attribution 3.0 Unported License. [<http://dx.doi.org/10.1063/1.4870759>]

Functional properties of semiconductors,¹ multiferroics,² ferroelectrics,³ ferromagnets⁴ and materials for data storage⁵ depend strongly on lattice parameters. Whereas in bulk lattice parameters are only changed by composition or temperature, in thin films, lattice parameters can be varied by coherent growth. For coherent film growth on single crystalline substrates, the in-plane lattice parameter of the film is determined by the substrate lattice parameter. Since a thin film often adapts both, in-plane lattice parameter and symmetry of the substrate, e.g., substrates with (001) orientation may be used to induce a tetragonal distortion within the film.

As this tetragonal distortion follows the Bain transformation,⁶ connecting a body-centred cubic (bcc) and face-centred cubic (fcc) structure, this is called the epitaxial Bain path: starting from the austenite (fcc) via fct (face-centred tetragonal) and bct (body-centred tetragonal) to bcc. By a geometric relationship of the fcc and bct unit cells—the a and b-axes of bct are rotated by 45° with respect to their fcc counterparts—all structures may be described with one parameter: the tetragonal distortion of the face centred unit cell (c/a_{fcc} ratio). Within this description, the fcc structure has no tetragonal distortion and c/a_{fcc} is 1. Along the Bain path the c/a_{fcc} ratio changes continuously from 1 for fcc to 0.71 for bcc. This approach was verified recently on the example of Fe-Pd(-X) magnetic shape memory alloys, where tetragonal distortion was varied between 0.77 and 1.09; resulting in huge variations of the magnetocrystalline anisotropy, Curie temperature, and saturation magnetization.^{7–9}

However, this approach is a time-consuming process since individual films on substrates with different lattice parameters have to be prepared and characterized. Though the use of coherent element buffer layers can expand the range of lattice constants, it remains a serial approach. The tetragonal distortion of the film is adjusted stepwise and not continuously. Thus, the optimum

^aE-mail: s.weiss@ifw-dresden.de

value can easily be missed. For the systematic compositional variation of a coherent buffer layer, combinatorial thin film preparation techniques are highly promising and offer a route to overcome this drawback.

Here, we demonstrate epitaxial binary alloy buffer layers with continuously graded in-plane lattice parameters. Using this technique, more than 300 samples are deposited on one 4-in. wafer.¹⁰ All samples on one wafer are defined as material library. Complete binary or ternary systems can be fabricated in one deposition process and systematically characterized by automated high-throughput methods.¹¹ As a binary buffer layer system we selected the Cu-Au system that exhibits a fcc disordered solid solution (Au,Cu) over the whole composition range at higher temperatures.¹² The lattice parameters lie between the values of the pure elements.¹³ The disordered solid solution can be stabilized by quenching from high temperatures to room temperature. Sputter deposition on substrates at ambient temperatures yields such high quenching rates.

In this paper, we analyze structure and texture of the Cu-Au layer on one 4-in. Si wafer with X-ray diffraction in dependency of the composition. The Cu-Au compositions are adjusted to a range, where their lattice parameters are promising for tuning the magnetic properties of materials systems such as Fe-Pd and Fe-Co. These Bain libraries will be of particular interest for rare-earth free permanent magnets based on Fe-Co,¹⁴ where theoretical calculations predict a strong influence of lattice strain on the magnetocrystalline anisotropy.^{5,15}

Cu-Au thin film Bain libraries with 50 to 90 at. % Cu were prepared using a combinatorial magnetron sputtering system (CMS 600/400LIN, DCA). The composition gradient was obtained by co-sputtering from element targets (100 mm diameter, purity 99.99%) on a (001) oriented 4-in. Si wafer. The angle between the targets in the sputtering chamber is 144°, which results in material libraries with a small thickness gradient (40 nm–45 nm) as well as a large composition gradient. The base pressure was below 8.5×10^{-8} mbar. The Bain library was deposited at room temperature with an Ar sputter pressure of 2.7 mbar, the sputter rates were 0.044 nm/s for Cu and 0.019 nm/s for Au. Before deposition of the Cu-Au layer, the Si wafer was coated with a photoresist grid (Micro-Chemicals AZ 1518) and structured into an array of discrete 3×3 mm² squares using a lift-off process. Afterwards, the Si wafer was etched with a buffered 9% hydrofluoric acid solution for several minutes to remove the native SiO₂ on top of the wafer. Prior the deposition of the Cu-Au library on the Si wafer, two thin buffer layers were deposited. A 5 nm Cu layer (0.044 nm/s) was deposited directly on the Si wafer to improve adhesion, followed by a 10 nm Pd layer (0.05 nm/s) to reduce misfits between Cu and Cu_{100-x}Au_x and to improve the quality of film growth. After deposition, the photoresist between the discrete 3×3 mm² squares was removed by a lift-off step.

High-throughput X-ray diffraction (XRD) measurements (X'Pert PRO X-ray diffractometer PANalytical equipped with a PIXcel line detector, Bragg–Brentano geometry, Cu-K α radiation) were performed to determine the structure of the Cu-Au Bain library at room temperature. With texture measurements in a four-circle setup (X'Pert, Cu-K α radiation) the orientation relationship was investigated and visualised using custom made software.¹⁶ The compositions were mapped by automated energy dispersive X-ray (EDX) spectroscopy (Jeol JSM 5800 equipped with an Oxford Inca EDX system, systematic error 1 at. %) and verified with Rutherford Backscattering spectrometry (RBS, incident He⁺ 1.7 MeV, detector angle 170°, circular spot of 1 mm diameter, systematic error 0.2 at. %) on selected samples. The film thickness was determined by a mechanical profilometer measuring the step between the substrate surface and film surface created by the lift-off step. The film roughness was determined by Atomic Force Microscope (AFM) measurements using a Digital Instruments Dimension 3100 microscope.

We focus on the composition range of Cu-Au, where in-plane lattice parameters are predicted to induce best magnetic properties in Fe-Pd^{8,9} and Fe-Co.^{5,14,15} From bulk experiments it is known that more than 50 at. % Cu are necessary to achieve lattice parameters between 0.365 nm and 0.39 nm.¹³

Quantitative element depth profiling of selected 3×3 mm² samples was done by use of RBS. In Fig. 1 results of two exemplary samples are shown: The first contains a high amount of Cu as it was located close to the Cu target during deposition (Fig. 1(a)). The second contains less Cu since it was closer to the Au target during deposition (Fig. 1(b)). The simulated positions of the different elements are colour coded. In the low energy end of the spectrum (channels below 520)

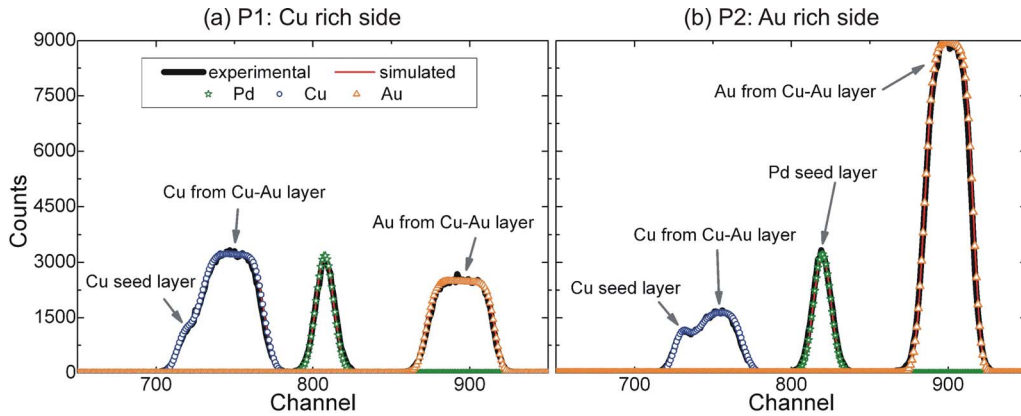


FIG. 1. RBS spectra of a Cu rich sample (point 1, (a)) and an Au rich sample (point 2, (b)). The simulated peaks of the different elements are colour coded. For Cu, two peaks are visible originating from the different layers.

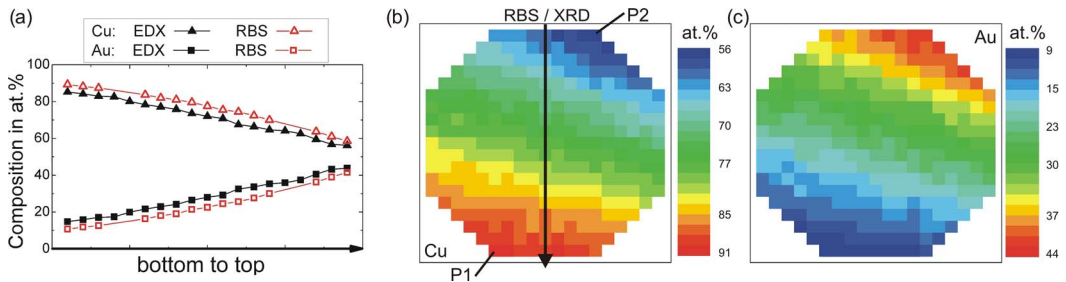


FIG. 2. (a) Comparison of RBS and EDX scans of Au-Cu buffer deposited on Si(001)/5 nm Cu/10 nm Pd. EDX measurements give systematically lower values for the Cu content. The error is in the range of the symbol size. RBS corrected EDX composition mapping of Cu (b) and Au (c). An in-plane Cu gradient across the Bain library from 91 (bottom edge) to 56 at. % (top edge) was obtained.

the backscattered signal from the Si substrate occurs (not shown). Between channels from 790 to 820 the Pd from the seed layer is visible. The peak between 850 and 930 originates from Au within the Cu-Au layer. Two Cu signals occur between channels from 700 to 770: a very prominent (main) peak originating from the Cu-Au layer and on its left side a shoulder from the Cu seed layer. The ratio of counts between the main Cu and the Au peak determine the Cu-Au ratio.

An automated EDX mapping gives the composition of all $3 \times 3 \text{ mm}^2$ sample points of the Bain library. However, EDX measurements are not only sensitive to a thin surface layer. The 5 nm Cu seed layer and the 10 nm Pd layer also contribute to the EDX signal. EDX measurements give systematically lower values for the Cu content. Nevertheless, the EDX map shows a large change of the Cu content across the library (Fig. 2(b)). By correcting with the offset from RBS, the composition over the wafer area varies from $\text{Cu}_{56}\text{Au}_{44}$ (P2) to $\text{Cu}_{91}\text{Au}_9$ (P1).

XRD measurements in Bragg-Brentano geometry were performed on all $3 \times 3 \text{ mm}^2$ sample points to determine the structure and the buffer lattice parameters. The arrow in Fig. 2(b) tags the corresponding sample points corresponding to the diffraction patterns depicted in Fig. 3. The $\text{Cu-Au}\{002\}$ reflection is located between the $\{002\}$ diffraction peaks of the pure elements Cu and Au and shifts to higher angles with increasing Cu content. In addition to the $\{002\}$ reflection a minor $\{111\}$ reflection occurs between the $\{111\}$ reflections of the pure elements. As a measure for the degree of texture one can use the intensity ratio of both reflections. For all compositions the $\{002\}$ reflection appears with a higher intensity than the $\{111\}$ reflection. The ratio of I_{002}/I_{111} is at least 4:1 which is much higher than the ratio of 1:3 of an untextured film. The lowest values of the intensity ratio are around 75 at. % Cu.

The out-of-plane coherence length, determined from the full width at half maximum (FWHM), of all sample points is 15 nm on average. With increasing Au content, the coherence length only

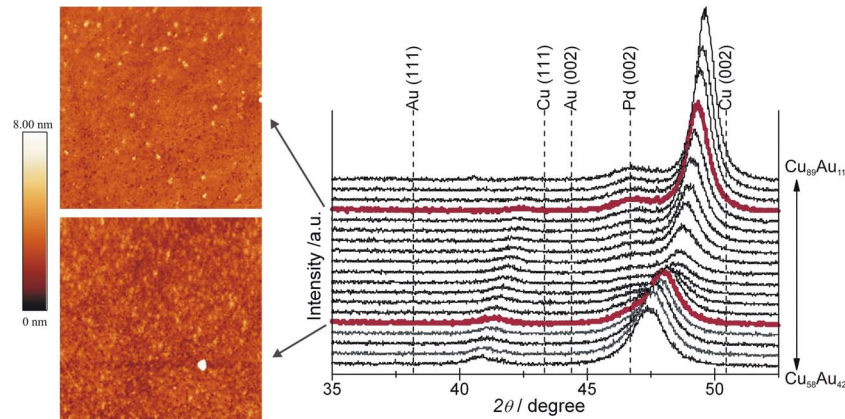


FIG. 3. Bragg-Brentano scans along the Cu-Au gradient (arrow in Fig. 2(b)). Reflection positions of the pure elements are marked by vertical lines. For all Cu-Au compositions a weak {002} reflection of the Pd seed layer is visible. The {002} Cu-Au reflection is much stronger than the {111} reflection. With increasing Cu content the {002} and the minor {111} reflection is shifted to higher 2θ -values—closer to the {002} of pure Cu. Atomic force micrographs for two selected samples ($\text{Cu}_{86}\text{Au}_{14}$ and $\text{Cu}_{86}\text{Au}_{32}$) marked in red, show a rather smooth surface without any hints for crystal grains.

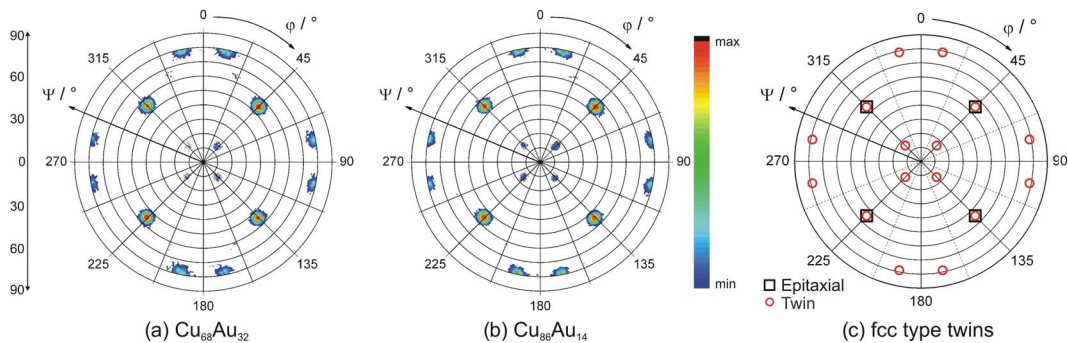


FIG. 4. {111} pole figures of (a) $\text{Cu}_{68}\text{Au}_{32}$ and (b) $\text{Cu}_{86}\text{Au}_{14}$, and (c) simulation of {111}(11-2) fcc type deformation/growth twins. The main intensities at $\Phi = n \cdot 45^\circ$ and $\Psi = 54^\circ$ originate from epitaxially grown Au-Cu. Additional intensities occur from fcc type twinning.

slightly decreases and thus the quality of coherent growth. Pure Au only grows coherently on MgO at elevated temperatures in the range of 300°C . This is attributed to the high surface energy of (001) Au, which favours (111) oriented growth. Further it is known that Cu grows very well coherently on MgO substrates at room temperature.⁷ Both effects contribute to a broadening of the (002) reflection and thus a decrease of coherence length with increasing Au content.

For sample points around 75 at. % Cu, the FWHM scatters slightly. From the phase diagram is known that Cu-Au transforms into ordered structures at certain temperatures:¹² L_{12} and L_{10} . The L_{10} transformation is suppressed by quenching, which is realized by depositing at room temperature. However, the L_{12} transformation cannot be suppressed completely. The XRD pattern does not show any superstructure reflections. Since XRD probes only long range order, short range order may not be excluded.

In order to prove epitaxial growth texture measurements were performed using the Si substrate as an absolute reference frame. Figure 4 shows two pole figures of the {111} reflection for two samples along the Cu-Au gradient, one with 68 at. % Cu (Fig. 4(a)) and one with 86 at. % Cu (Fig. 4(b)). In Fig. 4, the Si edge of [100] is oriented 45° to the edges of the figure. The four main intensities at a sample tilt angle $\Psi = 54.7^\circ$ and a rotation angle $\Phi = n \cdot 45^\circ$ originate from the coherently grown Cu-Au layer. This means that (002) plane is oriented parallel to the film surface, in agreement with the Bragg-Brentano scans. (200) and (020) planes are aligned perpendicular to the film surface. Since the maximum intensities occur at rotation angles of $\Phi = n \cdot 45^\circ$ the a -axis of

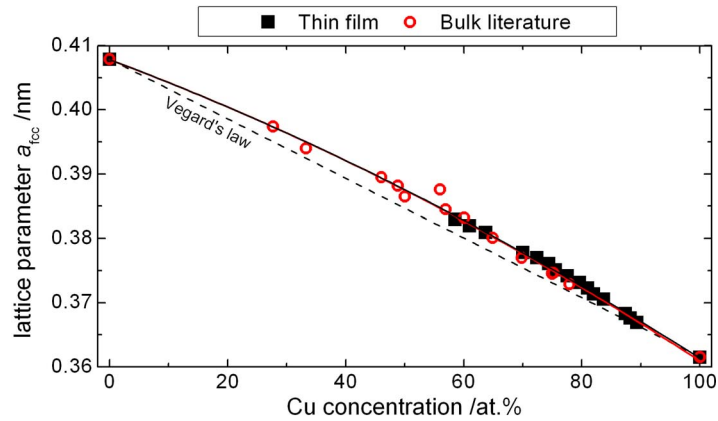
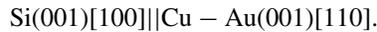


FIG. 5. The calculated lattice parameter a_{fcc} of the disordered Cu-Au unit cell agrees well with literature values observed in quenched bulk materials.¹³ The error is in the range of the symbol size.

Cu-Au is rotated 45° relative to the a -axis of Si. This reveals an orientation relationship between the Cu-Au unit cell and the Si substrate as follows:



The additional intensities in the $\{111\}$ pole figures (Fig. 4) do not originate from the epitaxially grown Cu-Au. Following pole figure simulations,¹⁷ a $\{111\}\langle 11-2 \rangle$ fcc type deformation/growth twinning process in Cu-Au is identified as origin for their appearance. A reason for the formation of deformation/growth twins is high elastic stresses during the epitaxial film growth. By changing the sputter power or the angle between target and substrate one may be able to decrease the energy during deposition and thus the stress.

Since counts of the twin poles are $<20\%$ of the epitaxial $\{111\}$ intensity, we conclude that 40 nm Cu-Au grows mainly undisturbed and epitaxially. Additional AFM measurements (Fig. 3) reveal a flat surface morphology. Thin film roughness on the Cu rich buffers is low in general and increases towards higher Au contents. Typical values for the root-mean square roughness (RMS) are 0.5 nm for $\text{Cu}_{86}\text{Au}_{14}$ and 1.1 nm for $\text{Cu}_{68}\text{Au}_{24}$.

The lattice parameters a_{fcc} of the Cu-Au layer were calculated from the $\{002\}$ reflection positions measured in Bragg-Brentano geometry. The results are plotted in Fig. 5. With increasing Cu content, a_{fcc} is decreasing significantly. Our results agree well with the trend observed in quenched, polycrystalline bulk materials.¹³ For both, bulk and thin films, a positive deviation from Vegard's law of a mixed crystal occurs.^{13,18} The thickness of the Cu-Au buffer layers is in a way that the Cu-Au exhibits the (relaxed) lattice parameter of bulk samples. As the Cu-Au layer is continuous and dense, a further increase of thickness is not necessary.

In conclusion, high quality buffer layers covering a compositional range from $\text{Cu}_{56}\text{Au}_{44}$ to $\text{Cu}_{91}\text{Au}_9$ were fabricated, exhibiting a continuous variation of lattice parameter from 0.365 nm to 0.382 nm. This covers the interesting range for both, Fe-Co-X and Fe-Pd-X. For the latter, an in-plane lattice parameter a_{fcc} around 0.375 nm is necessary to induce highest magnetocrystalline anisotropy.⁹ However, with the proposed method, one can tune the lattice parameter of the layer over the whole range between the lattice parameters of the pure elements Cu and Au.

This exemplary Bain library illustrates the lateral variation of lattice parameter on wafer scale. This approach may also be used for other binary systems which form solid solutions without formation of intermetallic phases. For cost reasons, Si wafers are the preferred substrates—as their size is large enough for combinatorial fabrication as well as high-throughput and detailed examinations of structure and properties of the functional layer on top. It expands the parameters available for combinatorial material science towards coherent growth with a large variation of lattice parameters, which is a key parameter for novel functional materials. High-throughput methods can be used for both, preparation and characterization, which will accelerate the search for novel materials in a short time frame.

The authors thank B. Eichler, A. Backen, A. Diestel, C. Behler, and R. Niemann for discussions and experimental support and the DFG for funding via the Priority Program SPP 1239 and the EU for funding via REFREPERMAG-FP7.

- ¹J. C. Bean, *Science* **230**, 127 (1985).
- ²J. Wang, J. B. Neaton, H. Zheng, V. Nagarajan, S. B. Ogale, B. Liu, D. Viehland, V. Vaithyanathan, D. G. Schlom, U. V. Waghmare, N. A. Spaldin, K. M. Rabe, M. Wuttig, and R. Ramesh, *Science* **299**, 1719 (2003).
- ³C. Ederer and N. A. Spaldin, *Phys. Rev. Lett.* **95**, 257601 (2005).
- ⁴A. Winkelmann, M. Przybylski, F. Luo, Y. Shi, and J. Barthel, *Phys. Rev. Lett.* **96**, 257205 (2006).
- ⁵T. Burkert, L. Nordström, O. Eriksson, and O. Heinonen, *Phys. Rev. Lett.* **93**, 027203 (2004).
- ⁶E. C. Bain, *Trans. Am. Inst. Min., Metall. Eng.* **70**, 25 (1924).
- ⁷S. Kauffmann-Weiss, M. E. Gruner, A. Backen, L. Schultz, P. Entel, and S. Fähler, *Phys. Rev. Lett.* **107**, 206105 (2011).
- ⁸J. Buschbeck, I. Opahle, M. Richter, U. K. Rößler, P. Klaer, M. Kallmayer, H. J. Elmers, G. Jakob, L. Schultz, and S. Fähler, *Phys. Rev. Lett.* **103**, 216101 (2009).
- ⁹S. Kauffmann-Weiss, S. Hamann, M. E. Gruner, L. Schultz, A. Ludwig, and S. Fähler, *Acta Mater.* **60**, 6920–6930 (2012).
- ¹⁰A. Ludwig, R. Zarnetta, S. Hamann, A. Savan, and S. Thienhaus, *Int. J. Mater. Res.* **99**, 1144–1149 (2008).
- ¹¹S. Thienhaus, S. Hamann, and A. Ludwig, *Sci. Technol. Adv. Mater.* **12**, 054206 (2011).
- ¹²H. Okamoto, D. J. Shakrabarti, D. E. Laughlin, and T. B. Massalski, *Bull. Alloy Phase Diagrams* **8**, 454 (1987).
- ¹³W. B. Pearson, *Handbook of Lattice Spacing and Structures of Metals and Alloys* (Oxford Pergamon Press, 1958), pp. 411 and 601.
- ¹⁴F. Yildiz *et al.*, *Phys. Rev. B* **80**, 064415 (2009).
- ¹⁵C. Neise, S. Schönecker, M. Richter, K. Koepf, and H. Eschrig, *Phys. Status Solidi B* **248**, 2398 (2011).
- ¹⁶A. Kauffmann, 2011 CorrVert, see <http://sco.ifw-dresden.de/xpert/CorrVert.html>.
- ¹⁷S. Kauffmann-Weiss, A. Kauffmann, R. Niemann, J. Freudenberger, L. Schultz, and S. Fähler, *Metals* **3**, 319–336 (2013).
- ¹⁸H. E. v. Steinwehr, *Z. Kristallogr.* **125**, 360 (1967).